CO$_2$ Adsorption on PtCu Sub-Nanoclusters Deposited on Pyridinic N-Doped Graphene: A DFT Investigation

Fernando Montejo-Alvaro [1], Diego González-Quijano [2], Jorge A. Valmont-Pineda [3], Hugo Rojas-Chávez [4], José M. Juárez-García [5], Dora I. Medina [6,*] and Heriberto Cruz-Martínez [1,*]

1   Tecnológico Nacional de México, Instituto Tecnológico del Valle de Etla, Abasolo S/N, Barrio del Agua Buena, Santiago Suchilquitongo, Oaxaca 68230, Mexico; moaf1217@gmail.com
2   Centro de Ciencias de la Ingeniería, Universidad Autónoma de Aguascalientes Campus sur, Av. Prolongación Mahatma Ghandi 6601, Colonia el Gigante 20340, Aguascalientes, Mexico; diegoxjgq@gmail.com
3   Tecnológico Nacional de México, Instituto Tecnológico del Istmo, Panamericana 821, 2da., Juchitán de Zaragoza, Oaxaca 70000, Mexico; jorge.vp@itistmo.tecnm.mx
4   Tecnológico Nacional de México, Instituto Tecnológico de Tláhuac II, Camino Real 625, Tláhuac, Ciudad de México 13508, Mexico; rojas_hugo@ittlahuac2.edu.mx
5   Universidad Tecnológica del Estado de Querétaro, Av. Pie de la Cuesta 2501, Nacional, Santiago de Querétaro, Querétaro 76148, Mexico; josman_jg@yahoo.com.mx
6   Tecnologico de Monterrey, School of Engineering and Sciences, Atizapan de Zaragoza 52926, Estado de Mexico, Mexico
*   Correspondence: dora.medina@tec.mx (D.I.M.); heri1234@hotmail.com (H.C.-M.)

Abstract: To reduce the CO$_2$ concentration in the atmosphere, its conversion to different value-added chemicals plays a very important role. Nevertheless, the stable nature of this molecule limits its conversion. Therefore, the design of highly efficient and selective catalysts for the conversion of CO$_2$ to value-added chemicals is required. Hence, in this work, the CO$_2$ adsorption on Pt$_{4-x}$Cu$_x$ (x = 0–4) sub-nanoclusters deposited on pyridinic N-doped graphene (PNG) was studied using the density functional theory. First, the stability of Pt$_{4-x}$Cu$_x$ (x = 0–4) sub-nanoclusters supported on PNG was analyzed. Subsequently, the CO$_2$ adsorption on Pt$_{4-x}$Cu$_x$ (x = 0–4) sub-nanoclusters deposited on PNG was computed. According to the binding energies of the Pt$_{4-x}$Cu$_x$ (x = 0–4) sub-nanoclusters on PNG, it was observed that PNG is a good material to stabilize the Pt$_{4-x}$Cu$_x$ (x = 0–4) sub-nanoclusters. In addition, charge transfer occurred from Pt$_{4-x}$Cu$_x$ (x = 0–4) sub-nanoclusters to the PNG. When the CO$_2$ molecule was adsorbed on the Pt$_{4-x}$Cu$_x$ (x = 0–4) sub-nanoclusters supported on the PNG, the CO$_2$ underwent a bond length elongation and variations in what bending angle is concerned. In addition, the charge transfer from Pt$_{4-x}$Cu$_x$ (x = 0–4) sub-nanoclusters supported on PNG to the CO$_2$ molecule was observed, which suggests the activation of the CO$_2$ molecule. These results proved that Pt$_{4-x}$Cu$_x$ (x = 0–4) sub-nanoclusters supported on PNG are adequate candidates for CO$_2$ adsorption and activation.

Keywords: CO$_2$ adsorption; adsorption energy; charge transfer; stability

1. Introduction

Due to human activity associated with the usage of fossil fuels and industrialization, the concentration of CO$_2$ in the atmosphere has increased considerably. It is causing environmental problems such as the greenhouse effect, global warming, and climate change among others [1–3]. Therefore, in order to reduce the CO$_2$ concentration in the atmosphere, various investigations and technologies are being developed such as the CO$_2$ sequestration process [4,5], and CO$_2$ conversion into different value-added chemicals is another strategy widely used [6–8]. Nevertheless, the stable nature of the CO$_2$ molecule limits its conversion [9,10]. Therefore, the design of highly efficient and selective catalysts for the conversion of CO$_2$ into value-added chemicals is required.

Currently, many catalysts have been designed for CO_2 conversion into value-added chemical products, among them the transition metal nanoparticles-based catalysts can be highlighted [11,12]. However, more recently, it has been documented that alloy catalysts have more outstanding catalytic activities than monometallic nanoparticles for CO_2 conversion [13,14]. Among the different bimetallic catalysts studied, PtCu nanoparticles have become very important because they present good catalytic properties for the CO_2 conversion [15–17]. For example, Cu–Pt alloy nanocubes with a relatively broad range of composition ratios were synthesized and evaluated for CO_2 electroreduction reaction [15]. It was found that the Cu–Pt alloys exhibit compositional-dependent activities towards CO_2 electroreduction. In another study, Cu–Pt nanocrystals with different amounts of Cu and Pt were prepared and evaluated for CO_2 electroreduction reaction [16]. Guo and coworkers highlighted the importance of the compositional effect of Cu–Pt nanocrystals on their catalytical activities in what CO_2 electroreduction is concerned. In addition, it was demonstrated that the Cu–Pt (3:1) nanocrystals exhibited the highest activity and faradaic efficiency in the CO_2 electroreduction reaction among all the as-prepared Cu–Pt samples. Recently, a density functional theory (DFT) study of CO_2 adsorption on $Cu_{4-x}Pt_x$ (x = 0–4) clusters was performed [18]. It was computed that the gas phase linear CO_2 molecule was deformed upon adsorption, with its bend angle varying from about 134° to 145°, which could favor the CO_2 dissociation. It can be inferred from these studies that Cu–Pt alloys are good candidates for the conversion of CO_2 to value-added products.

However, it is well known that metallic nanoparticles tend to agglomerate due to their high surface energies, which in turn involves the coarsening of larger particles from those of smaller size [19,20]. Therefore, to overcome the agglomeration problems, it is necessary to disperse or support these nanoparticles on materials with high surface area. To this end, graphene is considered a good support material due to its high specific surface area, excellent electrical conductivity, and resistance to corrosion [21,22], however, this material has a limited chemical reactivity [23]. Consequently, various approaches have been implemented to improve its activity, e.g., functionalization and doping among others [24–26]. Specifically, among the different dopants used to modify graphene reactivity, pyridinic-type N doping can be highlighted because it enhances both the stability and reactivity of metallic nanoparticles [27,28]. Nowadays, there is a sizeable number of theoretical studies that analyze the stability and reactivity of metal nanoparticles supported on pyridinic N-doped graphene (PNG) [29–31]. These studies show the potential of PNG to improve not only the stability, but also the reactivity of metal nanoparticles for different applications [29–31].

According to the literature, the reactivity and stability of $Pt_{4-x}Cu_x$ (x = 0–4) clusters supported on PNG substrate was investigated using the DFT [32]. It was demonstrated that Pt–Cu nanoparticles supported on PNG are good candidates to adsorb the glyphosate molecule and PNG stabilized the Pt–Cu nanoparticles as well [32]. However, to the best of our knowledge, there are no theoretical studies on CO_2 adsorption on Pt–Cu clusters supported on PNG using the DFT calculations. Therefore, in this work, the CO_2 adsorption on Pt–Cu sub-nanoclusters deposited on PNG was studied using the DFT calculations. In order to achieve this goal, the most stable interaction between the $Pt_{4-x}Cu_x$ (x = 0–4) sub-nanoclusters and the PNG was investigated. Furthermore, DFT calculations were used to bring light into the CO_2 adsorption on $Pt_{4-x}Cu_x$ (x = 0–4) sub-nanoclusters deposited on PNG.

2. Computational Methodology

All calculations were carried out within the DFT implemented in the ORCA 5.0.0 package [33]. All the electronic structure calculations were addressed through the revised Perdew–Burke–Ernzerhof exchange correlation functional (revPBE) [34]. For the C, H, N, and O atoms, the Ahlrichs basis sets def2-SVP were used for the calculations and def2-TZVP for the Cu atoms [35], whereas the Pt ones were treated using the basis set LANL2DZ for effective core potentials [36]. The convergence tolerances for geometry optimization were energy

change = 5×10^{-6} Eh, max. gradient = 3×10^{-4} Eh/Bohr, rms gradient = 1×10^{-4} Eh/Bohr, max. displacement = 4×10^{-3} Bohr, and rms displacement = 2×10^{-3} Bohr.

To investigate the stability of $Pt_{4-x}Cu_x$ (x = 0–4) sub-nanoclusters on PNG, the most stable structures for the $Pt_{4-x}Cu_x$ (x = 0–4) sub-nanoclusters were obtained from a previous study [18]. However, it is worth highlighting that these structures were reoptimized employing the methodology used in this study, which are depicted in Figure 1.
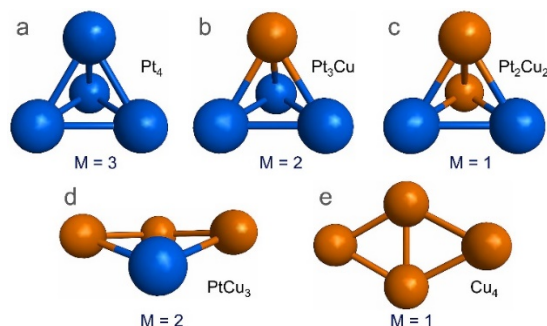

Figure 1. Structures and spin multiplicity (M) of $Pt_{4-x}Cu_x$ (x = 0–4) sub-nanoclusters. (**a**) Pt_4, (**b**) Pt_3Cu, (**c**) Pt_2Cu_2, (**d**) $PtCu_3$, and (**e**) Cu_4.

The pyridinic-type N doping can be located anywhere on the graphene (e.g., edge or center). Here, we used graphene as the support material, therefore, the doping was localized in the center of the graphene. In this case, different numbers of nitrogen atoms (e.g., 1, 2, or 3) can be used. In this work, we used pyridinic-type doping with three N atoms, as it has been a widely used structure [29–31,37]. In this sense, circumcoronene ($C_{54}H_{18}$) was used as model of graphene. To obtain the PNG structure, a C atom was removed from the center of the graphene to create a vacancy, then the hanging C atoms were replaced by N ones, as shown in Figure 2.
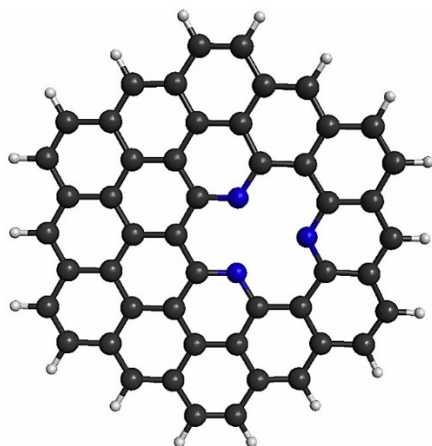

Figure 2. Pyridinic N_3-doped graphene structure.

The binding energies (E_b) between the $Pt_{4-x}Cu_x$ (x = 0–4) sub-nanoclusters and the PNG were calculated as follows:

$$E_b = E_{sub-nanocluster/PNG} - \left(E_{sub-nanocluster} + E_{PNG}\right) \tag{1}$$

where $E_{sub-nanocluster/PNG}$, $E_{sub-nanocluster}$, and E_{PNG} are the energies of the $Pt_{4-x}Cu_x$ (x = 0–4) sub-nanoclusters deposited on PNG, $Pt_{4-x}Cu_x$ (x = 0–4) sub-nanoclusters, and the PNG structure, respectively.

The adsorption energies (E_{ads}) of CO_2 on $Pt_{4-x}Cu_x$ (x = 0–4) sub-nanoclusters deposited on PNG were obtained as:

$$E_{ads} = E_{sub-nanocluster/PNG+CO_2} - \left(E_{sub-nanocluster/PNG} + E_{CO_2}\right) \tag{2}$$

where $E_{sub-nanocluster/PNG+CO_2}$ is the energy of CO_2 adsorbed on $Pt_{4-x}Cu_x$ (x = 0–4) sub-nanoclusters deposited on PNG, while $E_{sub-nanocluster/PNG}$ and E_{CO_2} are the energies as a single point calculation of the free-standing $Pt_{4-x}Cu_x$ (x = 0–4) sub-nanoclusters supported on PNG and the CO_2 molecule from the optimized structure of the $Pt_{4-x}Cu_x$ (x = 0–4)/PNG+CO_2 composite, respectively.

　　　To analyze the molecular interactions of the sub-nanoclusters supported on PNG and the CO_2 adsorption over $Pt_{4-x}Cu_x$ (x = 0–4) sub-nanoclusters deposited on PNG, the Quantum Theory of Atoms in Molecules (QTAIM) developed by Bader was employed for the charge transfer analyses; to this end, the Multiwfn program was used [38].

3. Results

3.1. Stability of $Pt_{4-x}Cu_x$ (x = 0–4) Sub-Nanoclusters on PNG

　　　The most stable interaction between $Pt_{4-x}Cu_x$ (n = 0–4) sub-nanoclusters and PNG was determined using several configurations. Figures 3 and 4 illustrate the most stable interactions between the $Pt_{4-x}Cu_x$ (n = 0–4) sub-clusters and PNG. It was found that the most stable interaction between the Pt_4 sub-cluster and the PNG was with a Pt atom trapped in the vacancy of the PNG, which is consistent with a previous study reported in literature [39]. It is also investigated that the most stable interaction between the Pt_3Cu sub-nanocluster and PNG is with a Pt atom trapped in the vacancy of the PNG. For the case of Pt_2Cu_2 sub-nanocluster deposited on PNG, two isoenergetic structures were found as the most stable structures, see Figure 3c,d. In the first structure, the interaction occurred with two Cu atoms joined with PNG, where one of the atoms is anchored in the vacancy, while in another structure located at only 0.05 eV above the most stable structure, the interaction is with one atom of Cu and one of Pt, in this case the Cu atom is anchored into the vacancy.
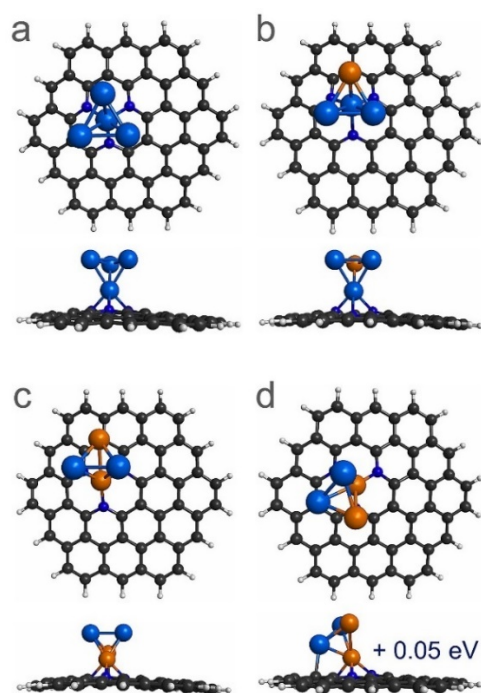

Figure 3. Top and side views of the most stable configurations of the adsorption of $Pt_{4-x}Cu_x$ (x = 0–2) sub-nanoclusters on PNG. (**a**) Pt_4/PNG, (**b**) Pt_3Cu/PNG, and (**c**,**d**) Pt_2Cu_2/PNG. Note that (**d**) is a quasi-degenerated state of the Pt_2Cu_2/PNG system with a difference in energy of 0.05 eV.
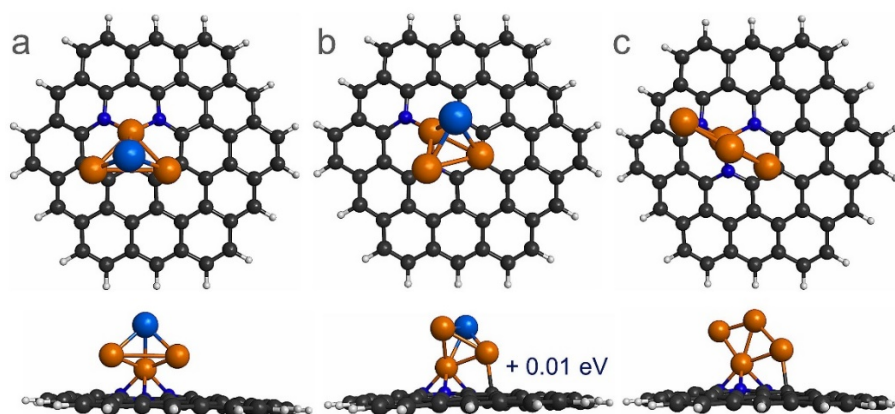
Figure 4. Top and side views of the most stable adsorption sites of $Pt_{4-x}Cu_x$ (x = 3 and 4) sub-nanoclusters on PNG. (**a,b**) $PtCu_3$/PNG and (**c**) Cu_4/PNG. Note that (**b**) is a quasi-degenerated state of the $PtCu_3$/PNG system with a difference in energy of 0.01 eV.

For $PtCu_3$ sub-nanoclusters supported on PNG, two isoenergetic configurations were also computed as the most stable structures, see Figure 4a,b. In the case of the most stable interaction, it is observed that the interaction between the $PtCu_3$ sub-nanoclusters and PNG occurred with three Cu atoms (Figure 4a), while in another structure, the interaction between the sub-nanocluster and the PNG occurred via two Cu atoms, see Figure 4b. Finally, for Cu_4 sub-nanocluster deposited on PNG, two Cu atoms interacted with the PNG. In addition, the E_b between the $Pt_{4-x}Cu_x$ (x = 0–4) sub-nanoclusters and the PNG were calculated, see Table 1. It is observed that E_b are substantially higher than those reported in previous findings for Pt-based sub-nanoclusters supported on pristine graphene [40,41]. Therefore, it can be inferred that PNG is a good support material for Pt-based nanoclusters. In addition, the calculated E_b between the Pt_4 and the PNG is −3.61 eV, which is similar to that reported in the literature with a value of −4.40 eV [39].

Table 1. Binding energies (E_b) and charge transfer between the $Pt_{4-x}Cu_x$ (x = 0–4) sub-nanoclusters and the PNG.

System	E_b (eV)	QTAIM Charge (e)
Pt_4/PNG	−3.61	0.23
Pt_3Cu/PNG	−3.01	0.26
Pt_2Cu_2/PNG	−2.65	0.52
$PtCu_3$/PNG	−3.26	0.69
Cu_4/PNG	−2.44	0.57

The interaction between the $Pt_{4-x}Cu_x$ (x = 0–4) sub-nanoclusters and PNG was further investigated by the QTAIM charge transfer, see Table 1. The results suggest that $Pt_{4-x}Cu_x$ (x = 0–4) sub-nanoclusters transfer charge to the PNG structure since these ended with a total positive charge, which can be attributed to the large electronegativity of the N atoms. Furthermore, it is observed that as the content of Cu in the sub-nanoclusters increases, the charge transfer from sub-nanoclusters to the PNG tends to increase as well, which can be attributed to the low electronegativity of the Cu atoms.

3.2. CO_2 Adsorption on $Pt_{4-x}Cu_x$ (x = 0–4) Sub-Nanoclusters Deposited on PNG

To analyze the adsorption and activation of the CO_2 molecule on the $Pt_{4-x}Cu_x$ (x = 0–4) sub-nanoclusters deposited on PNG, the CO_2 adsorption energy, CO_2 bond elongation, CO_2 bending angle, and charge transfer from sub-nanoclusters supported PNG to CO_2 were used as indicators of an effective CO_2 dissociation process [42,43]. To obtain the most stable interaction between the CO_2 and sub-nanoclusters supported PNG, several modes (e.g., top, bridge, and hollow) of CO_2 adsorption on sub-nanoclusters supported

on PNG were investigated. In Figure 5, the most stable CO_2 adsorption on the $Pt_{4-x}Cu_x$ (x = 0–4) sub-nanoclusters supported on the PNG is reported. The results show that the CO_2 molecule is deformed when it is adsorbed on the $Pt_{4-x}Cu_x$ (x = 0–4) sub-nanoclusters supported on PNG (Figure 5), giving way to a bending angle from 135.86° up to 141.25°, see Table 2. Similar results were obtained when the CO_2 molecule was adsorbed on $Cu_{4-x}Pt_x$ (x = 0–4) clusters [18]. In addition, it can be observed that the CO_2 is adsorbed side-on type on $Pt_{4-x}Cu_x$ (x = 1–4)/PNG composites, whereas for the Pt_4/PNG composite the CO_2 molecule is bonded with a Pt atom. The type of CO_2 adsorption on $Pt_{4-x}Cu_x$ (x = 1–4)/PNG composites is like those computed on $Cu_{4-x}Pt_x$ (x = 0–4) clusters [18]. To estimate the E_{ads} between the CO_2 molecule and the $Pt_{4-x}Cu_x$ (x = 0–4) sub-nanoclusters deposited on the PNG, the E_{ads} were calculated using Equation (2). It is observed that CO_2 presented a chemisorption on $Pt_{4-x}Cu_x$ (x = 0–4) sub-nanoclusters deposited on PNG, since in all cases the E_{ads} were higher than 1 eV. In addition, the CO_2 molecule is adsorbed stronger on bimetallic $Pt_{4-x}Cu_x$ (x = 1–4) sub-nanoclusters deposited on PNG than on Pt_4 sub-nanocluster supported on PNG, which can be attributed to the presence of Cu atoms in bimetallic sub-nanoclusters. Moreover, an elongation of the average C-O bond length is observed when the CO_2 is adsorbed on $Pt_{4-x}Cu_x$ (x = 0–4) sub-nanoclusters deposited on PNG (Table 2). It is worth noting that the free CO_2 presents an average C-O bond length of 1.20 Å. Considering the bond length elongation and the bending angle of the CO_2 molecule adsorbed on $Pt_{4-x}Cu_x$ (x = 0–4) sub-nanoclusters deposited on PNG, it is observed that there is an activation of the CO_2 molecule, which suggests that less energy is required to achieve the dissociation of this molecule. Finally, when CO_2 is adsorbed on $PtCu_3$ and Cu_4 sub-nanoclusters deposited on PNG, the structures of the $PtCu_3$ and Cu_4 sub-nanoclusters presented a deformation. For instance, the structure of the Cu_4 sub-nanocluster changes from planar to tetrahedral.
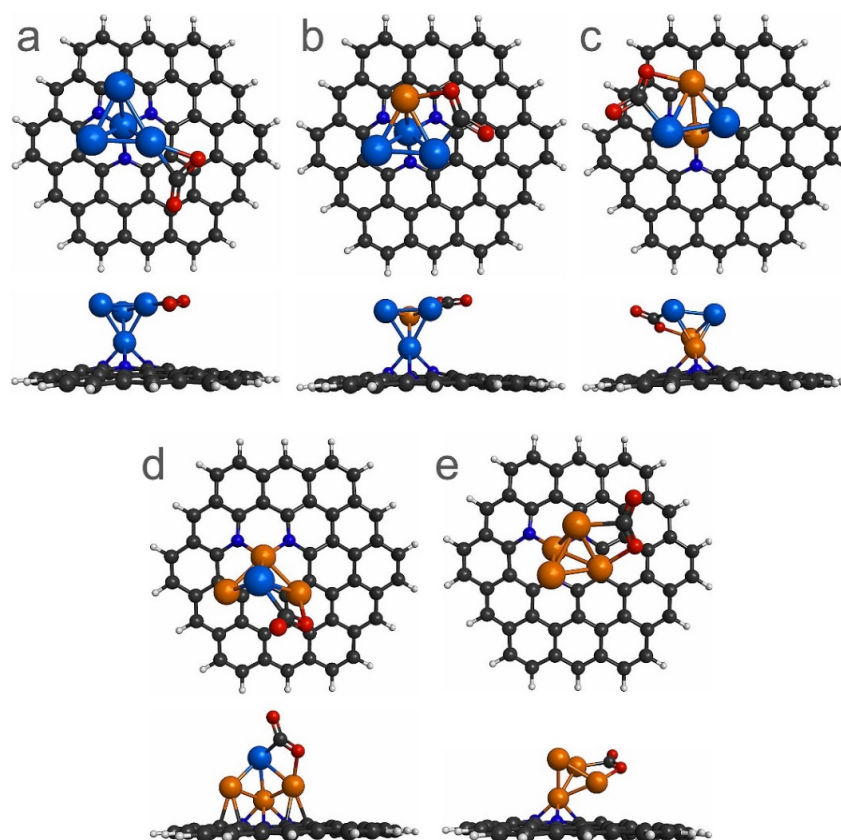

Figure 5. Top and side views of the most stable CO_2 adsorption sites on the sub-nanoclusters supported on the PNG: (**a**) Pt_4, (**b**) Pt_3Cu, (**c**) Pt_2Cu_2, (**d**) $PtCu_3$, and (**e**) Cu_4.

Table 2. Properties of the CO_2 adsorption on the $Pt_{4-x}Cu_x$ (x = 0–4) sub-nanoclusters supported on PNG.

System	E_{ads} (eV)	Charge Transfer Toward CO_2 (e)	Average CO_2 Bond Length (Å)	Bending Angle of CO_2 (°)
$CO_2/Pt_4/PNG$	−1.06	−0.37	1.24	141.25
$CO_2/Pt_3Cu/PNG$	−2.21	−0.42	1.24	140.03
$CO_2/Pt_2Cu_2/PNG$	−2.34	−0.44	1.25	139.32
$CO_2/PtCu_3/PNG$	−2.48	−0.46	1.25	135.86
$CO_2/Cu_4/PNG$	−1.81	−0.58	1.24	138.27

Finally, Table 2 shows the charge transfer between the CO_2 molecule and the $Pt_{4-x}Cu_x$ (x = 0–4) sub-nanoclusters supported on the PNG. The total charge of the CO_2 molecule resulted in negative values for all the systems studied, which indicated that the CO_2 molecule gained charge after the adsorption. Furthermore, it is observed that as the Cu content in the sub-nanoclusters increases, the charge transfer from the sub-nanoclusters supported on PNG to CO_2 molecule tends to increase as well, which can be attributed to the low electronegativity of the Cu atoms. Moreover, it is found that the charge transfer plays a significant role in the activation of the CO_2 molecule [42,43].

4. Conclusions

The CO_2 adsorption on the $Pt_{4-x}Cu_x$ (x = 0–4) sub-nanoclusters deposited on PNG was studied using the density functional theory. To the best of our knowledge, this is the first study on the CO_2 adsorption on the $Pt_{4-x}Cu_x$ (x = 0–4) sub-nanoclusters supported on PNG. First, the stability of the $Pt_{4-x}Cu_x$ (x = 0–4) sub-nanoclusters supported on PNG was analyzed. The results revealed that PNG enhanced the stability of the $Pt_{4-x}Cu_x$ (x = 0–4) sub-nanoclusters. After, the CO_2 adsorption on the $Pt_{4-x}Cu_x$ (x = 0–4) sub-nanoclusters deposited on PNG was computed. Numerous indicators such as E_{ads}, average bond length elongation, angle bending, and charge transfer were used to characterize the CO_2 interaction on the proposed systems. When the CO_2 molecule was adsorbed on the $Pt_{4-x}Cu_x$ (x = 0–4) sub-nanoclusters supported on the PNG, the CO_2 underwent both bond length elongation and bending angle. In addition, the charge transfer from the $Pt_{4-x}Cu_x$ (x = 0–4) sub-nanoclusters supported on PNG to the CO_2 molecule was observed. The results obtained with those indicators suggest that the activation of the CO_2 molecule took place. Therefore, the $Pt_{4-x}Cu_x$ (x = 0–4) sub-nanoclusters supported on PNG are suitable candidates for the CO_2 adsorption and activation.

Author Contributions: Conceptualization, F.M.-A., H.R.-C., D.I.M. and H.C.-M.; methodology, F.M.-A., D.G.-Q., J.A.V.-P., D.I.M. and H.C.-M.; formal analysis, F.M.-A., D.G.-Q., J.A.V.-P., H.R.-C., J.M.J.-G., D.I.M. and H.C.-M.; investigation, F.M.-A., D.G.-Q., J.A.V.-P., H.R.-C., J.M.J.-G., D.I.M. and H.C.-M.; writing—original draft preparation, F.M.-A., J.A.V.-P. and J.M.J.-G.; writing—review and editing, D.G.-Q., H.R.-C., D.I.M. and H.C.-M.; supervision, F.M.-A., D.I.M. and H.C.-M.; funding acquisition, F.M.-A. All authors have read and agreed to the published version of the manuscript.

Institutional Review Board Statement: Not applicable.

Informed Consent Statement: Not applicable.

Data Availability Statement: Not applicable.

References

1. Duan, X.; Xu, J.; Wei, Z.; Ma, J.; Guo, S.; Wang, S.; Liu, H.; Dou, S. Metal-free carbon materials for CO_2 electrochemical reduction. *Adv. Mater.* **2017**, *29*, 1701784. [CrossRef] [PubMed]
2. Wang, S.; Li, G.; Fang, C. Urbanization, economic growth, energy consumption, and CO_2 emissions: Empirical evidence from countries with different income levels. *Renew. Sustain. Energy Rev.* **2018**, *81*, 2144–2159. [CrossRef]
3. Bekun, F.V.; Emir, F.; Sarkodie, S.A. Another look at the relationship between energy consumption, carbon dioxide emissions, and economic growth in South Africa. *Sci. Total Environ.* **2019**, *655*, 759–765. [CrossRef] [PubMed]
4. Kemache, N.; Pasquier, L.C.; Cecchi, E.; Mouedhen, I.; Blais, J.F.; Mercier, G. Aqueous mineral carbonation for CO_2 sequestration: From laboratory to pilot scale. *Fuel Process. Technol.* **2017**, *166*, 209–216. [CrossRef]
5. Kaliyavaradhan, S.K.; Ling, T.C. Potential of CO_2 sequestration through construction and demolition (C&D) waste—An overview. *J. CO2 Util.* **2017**, *20*, 234–242. [CrossRef]
6. Nielsen, D.U.; Hu, X.M.; Daasbjerg, K.; Skrydstrup, T. Chemically and electrochemically catalysed conversion of CO_2 to CO with follow-up utilization to value-added chemicals. *Nat. Catal.* **2018**, *1*, 244–254. [CrossRef]
7. Gao, Y.; Qian, K.; Xu, B.; Li, Z.; Zheng, J.; Zhao, S.; Ding, F.; Sun, Y.; Xu, Z. Recent advances in visible-light-driven conversion of CO_2 by photocatalysts into fuels or value-added chemicals. *Carbon Resour. Convers.* **2020**, *3*, 46–59. [CrossRef]
8. Whang, H.S.; Lim, J.; Choi, M.S.; Lee, J.; Lee, H. Heterogeneous catalysts for catalytic CO_2 conversion into value-added chemicals. *BMC Chem. Eng.* **2019**, *1*, 9. [CrossRef]
9. Ma, J.; Sun, N.; Zhang, X.; Zhao, N.; Xiao, F.; Wei, W.; Sun, Y. A short review of catalysis for CO_2 conversion. *Catal. Today* **2009**, *148*, 221–231. [CrossRef]
10. Wang, W.; Wang, S.; Ma, X.; Gong, J. Recent advances in catalytic hydrogenation of carbon dioxide. *Chem. Soc. Rev.* **2011**, *40*, 3703–3727. [CrossRef]
11. Rahaman, M.; Dutta, A.; Broekmann, P. Size-dependent activity of palladium nanoparticles: Efficient conversion of CO_2 into formate at low overpotentials. *ChemSusChem* **2017**, *10*, 1733–1741. [CrossRef]
12. Dongare, S.; Singh, N.; Bhunia, H. Electrocatalytic reduction of CO_2 to useful chemicals on copper nanoparticles. *Appl. Surf. Sci.* **2021**, *537*, 148020. [CrossRef]
13. Bernal, M.; Bagger, A.; Scholten, F.; Sinev, I.; Bergmann, A.; Ahmadi, M.; Rossmeisl, J.; Cuenya, B.R. CO_2 electroreduction on copper-cobalt nanoparticles: Size and composition effect. *Nano Energy* **2018**, *53*, 27–36. [CrossRef]
14. Ismail, A.M.; Samu, G.F.; Balog, A.; Csapó, E.; Janáky, C. Composition dependent electrocatalytic behavior of Au–Sn bimetallic nanoparticles in carbon dioxide reduction. *ACS Energy Lett.* **2018**, *4*, 48–53. [CrossRef]
15. Zhao, X.; Luo, B.; Long, R.; Wang, C.; Xiong, Y. Composition-dependent activity of Cu–Pt alloy nanocubes for electrocatalytic CO_2 reduction. *J. Mater. Chem. A* **2015**, *3*, 4134–4138. [CrossRef]
16. Guo, X.; Zhang, Y.; Deng, C.; Li, X.; Xue, Y.; Yan, Y.M.; Sun, K. Composition dependent activity of Cu–Pt nanocrystals for electrochemical reduction of CO_2. *Chem. Commun.* **2015**, *51*, 1345–1348. [CrossRef] [PubMed]
17. Varela, A.S.; Schlaup, C.; Jovanov, Z.P.; Malacrida, P.; Horch, S.; Stephens, I.E.; Chorkendorff, I. CO_2 electroreduction on well-defined bimetallic surfaces: Cu overlayers on Pt (111) and Pt (211). *J. Phys. Chem. C* **2013**, *117*, 20500–20508. [CrossRef]
18. Gálvez-González, L.E.; Juárez-Sánchez, J.O.; Pacheco-Contreras, R.; Garzón, I.L.; Paz-Borbón, L.O.; Posada-Amarillas, A. CO_2 adsorption on gas-phase $Cu_{4-x}Pt_x$ (x= 0–4) clusters: A DFT study. *Phys. Chem. Chem. Phys.* **2018**, *20*, 17071–17080. [CrossRef]
19. Martínez-Espinosa, J.A.; Cruz-Martínez, H.; Calaminici, P.; Medina, D.I. Structures and properties of $Co_{13-x}Cu_x$ (x= 0–13) nanoclusters and their interaction with pyridinic N_3-doped graphene nanoflake. *Phys. E* **2021**, *134*, 114858. [CrossRef]
20. Rojas-Chávez, H.; Cruz-Martínez, H.; Flores-Rojas, E.; Juárez-García, J.M.; González-Domínguez, J.L.; Daneu, N.; Santoyo-Salazar, J. The mechanochemical synthesis of PbTe nanostructures: Following the Ostwald ripening effect during milling. *Phys. Chem. Chem. Phys.* **2018**, *20*, 27082–27092. [CrossRef]
21. Neto, A.C.; Guinea, F.; Peres, N.M.; Novoselov, K.S.; Geim, A.K. The electronic properties of graphene. *Rev. Mod. Phys.* **2009**, *81*, 109. [CrossRef]
22. Singh, V.; Joung, D.; Zhai, L.; Das, S.; Khondaker, S.I.; Seal, S. Graphene based materials: Past, present and future. *Prog. Mater. Sci.* **2011**, *56*, 1178–1271. [CrossRef]
23. Kong, X.K.; Chen, C.L.; Chen, Q.W. Doped graphene for metal-free catalysis. *Chem. Soc. Rev.* **2014**, *43*, 2841–2857. [CrossRef]
24. Montejo-Alvaro, F.; Rojas-Chávez, H.; Román-Doval, R.; Mtz-Enriquez, A.I.; Cruz-Martínez, H.; Medina, D.I. Stability of Pd clusters supported on pristine, B-doped, and defective graphene quantum dots, and their reactivity toward oxygen adsorption: A DFT analysis. *Solid State Sci.* **2019**, *93*, 55–61. [CrossRef]
25. Kaushal, S.; Kaur, M.; Kaur, N.; Kumari, V.; Singh, P.P. Heteroatom-doped graphene as sensing materials: A mini review. *RSC Adv.* **2020**, *10*, 28608–28629. [CrossRef]
26. Cruz-Martínez, H.; Rojas-Chávez, H.; Montejo-Alvaro, F.; Peña-Castañeda, Y.A.; Matadamas-Ortiz, P.T.; Medina, D.I. Recent Developments in Graphene-Based Toxic Gas Sensors: A Theoretical Overview. *Sensors* **2021**, *21*, 1992. [CrossRef] [PubMed]
27. Rangel, E.; Sansores, E. Theoretical study of hydrogen adsorption on nitrogen doped graphene decorated with palladium clusters. *Int. J. Hydrogen Energy* **2014**, *39*, 6558–6566. [CrossRef]
28. Rangel, E.; Sansores, E.; Vallejo, E.; Hernández-Hernández, A.; López-Pérez, P.A. Study of the interplay between N-graphene defects and small Pd clusters for enhanced hydrogen storage via a spill-over mechanism. *Phys. Chem. Chem. Phys.* **2016**, *18*, 33158–33170. [CrossRef]

29. Sánchez-Rodríguez, E.P.; Vargas-Hernández, C.N.; Cruz-Martínez, H.; Medina, D.I. Stability, magnetic, energetic, and reactivity properties of icosahedral M@ Pd$_{12}$ (M= Fe, Co, Ni, and Cu) core-shell nanoparticles supported on pyridinic N$_3$-doped graphene. *Solid State Sci.* **2021**, *112*, 106483. [CrossRef]

30. Wang, Q.; Tian, Y.; Chen, G.; Zhao, J. Theoretical insights into the energetics and electronic properties of MPt$_{12}$ (M= Fe, Co, Ni, Cu, and Pd) nanoparticles supported by N-doped defective graphene. *Appl. Surf. Sci.* **2017**, *397*, 199–205. [CrossRef]

31. Zhao, C.; Wu, H. Density functional investigation of mercury and arsenic adsorption on nitrogen doped graphene decorated with palladium clusters: A promising heavy metal sensing material in farmland. *Appl. Surf. Sci.* **2017**, *399*, 55–66. [CrossRef]

32. Gulati, A.; Kakkar, R. DFT study of adsorption of glyphosate pesticide on Pt-Cu decorated pyridine-like nitrogen-doped graphene. *J. Nanopart Res.* **2020**, *22*, 17. [CrossRef]

33. Neese, F. Software update: The ORCA program system, version 4.0. *Wiley Interdiscip Rev. Comput Mol. Sci.* **2018**, *8*, e1327. [CrossRef]

34. Zhang, Y.; Yang, W. Comment on "Generalized Gradient Approximation Made Simple". *Phys. Rev. Lett.* **1998**, *80*, 890. [CrossRef]

35. Weigend, F.; Ahlrichs, R. Balanced basis sets of split valence, triple zeta valence and quadruple zeta valence quality for H to Rn: Design and assessment of accuracy. *Phys. Chem. Chem. Phys.* **2005**, *7*, 3297. [CrossRef] [PubMed]

36. Hay, P.J.; Wadt, W.R. Ab initio effective core potentials for molecular calculations. Potentials for K to Au including the outermost core orbitale. *J. Chem. Phys.* **1985**, *82*, 299–310. [CrossRef]

37. Zhou, X.; Chu, W.; Sun, W.; Zhou, Y.; Xue, Y. Enhanced interaction of nickel clusters with pyridinic-N (B) doped graphene using DFT simulation. *Comput. Theor. Chem.* **2017**, *1120*, 8–16. [CrossRef]

38. Lu, T.; Chen, F. Multiwfn: A multifunctional wavefunction analyzer. *J. Comput. Chem.* **2012**, *33*, 580–592. [CrossRef]

39. Liu, S.; Huang, S. Theoretical insights into the activation of O$_2$ by Pt single atom and Pt$_4$ nanocluster on functionalized graphene support: Critical role of Pt positive polarized charges. *Carbon* **2017**, *115*, 11–17. [CrossRef]

40. Rêgo, C.R.; Tereshchuk, P.; Oliveira, L.N.; Da Silva, J.L. Graphene-supported small transition-metal clusters: A density functional theory investigation within van der Waals corrections. *Phys. Rev. B* **2017**, *95*, 235422. [CrossRef]

41. Fampiou, I.; Ramasubramaniam, A. Binding of Pt nanoclusters to point defects in graphene: Adsorption, morphology, and electronic structure. *J. Phys. Chem. C* **2012**, *116*, 6543–6555. [CrossRef]

42. Batista, K.E.; Ocampo-Restrepo, V.K.; Soares, M.D.; Quiles, M.G.; Piotrowski, M.J.; Da Silva, J.L. Ab Initio Investigation of CO$_2$ Adsorption on 13-Atom 4d Clusters. *J. Chem. Inf. Model.* **2020**, *60*, 537–545. [CrossRef] [PubMed]

43. Mendes, P.C.; Verga, L.G.; Da Silva, J.L. Ab initio screening of Pt-based transition-metal nanoalloys using descriptors derived from the adsorption and activation of CO$_2$. *Phys. Chem. Chem. Phys.* **2021**, *23*, 6029–6041. [CrossRef] [PubMed]